Sub-Nanosecond Tuning of Microwave Resonators Fabricated on Ruddlesden–Popper Dielectric Thin Films

Aaron M. Hagerstrom,* Xifeng Lu, Natalie M. Dawley, Hari P. Nair, Jordi Mateu, Robert D. Horansky, Charles A. E. Little, James C. Booth, Christian J. Long, Darrell G. Schlom, and Nathan D. Orloff

Voltage-tunable dielectric materials are widely used for microwave-frequency signal processing. Among tunable dielectric thin films, $(SrTiO_3)_n SrO$ Ruddlesden–Popper (RP) superlattices have exceptionally low loss at high frequencies. This paper reports the first realization of resonators, a ubiquitous building block of microwave components, fabricated on RP films, and an analysis of their static and dynamic tuning behavior. The RP film has a ferroelectric-paraelectric phase transition at ≈200 K, and the tunability is strongest at this temperature. The resonators have approximately 2.5% tuning of the resonance frequency at room temperature and 20% tuning at 200 K, and a tuning time scale of less than a nanosecond, which is limited by the measurement circuit rather than material properties.

Consumer demand for faster data rates and lower latencies is pushing the telecommunications industry to develop technologies that work at higher operating frequencies[1] with improved spectral efficiency. Tunable components are important for addressing these challenges. For example, tunable phase shifters are used in beamforming and multiple-input-multiple-output coding schemes in next-generation mobile handsets.[2–5] Ferroelectric materials have been widely studied

Dr. A. M. Hagerstrom, Dr. X. Lu, Prof. J. Mateu, Dr. R. D. Horansky, Dr. C. A. E. Little, Dr. J. C. Booth, Dr. C. J. Long, Dr. N. D. Orloff
Communications Technology Laboratory
National Institute of Standards and Technology
Boulder, CO 80305, USA
E-mail: Aaron.Hagerstrom@nist.gov
Dr. A. M. Hagerstrom, Dr. X. Lu
Department of Physics
University of Colorado
Boulder, CO 80309, USA
N. M. Dawley, Dr. H. P. Nair, Prof. D. G. Schlom
Department of Materials Science Engineering
Cornell University
Ithaca, NY 14853, USA
Prof. J. Mateu
Signal Theory and Communication Department
Universitat Politecnica de Catalunya
Castelldefels, Barcelona 08034, Spain
Dr. C. A. E. Little
Department of Mechanical Engineering
University of Colorado
Boulder, CO 80309, USA

as a way to build voltage-tunable devices.[6] Unfortunately, many of the most widely used tunable dielectrics have high loss at frequencies above 10 GHz,[7–10] which limits their usefulness in this frequency range. Notable exceptions are $(SrTiO_3)_n SrO$ Ruddlesden–Popper (RP) superlattices, which have an exceptionally low dielectric loss (tan $\delta \approx 0.05$ at 125 GHz)[10] at room temperature compared to other tunable dielectrics. In addition to the advantage of enabling low-loss devices, this low loss at mm-wave frequencies suggests another potential advantage of RP films. The lack of a relaxation frequency in the GHz range suggests that the material's dielectric constant can change on sub-nanosecond timescales. Fast tuning speeds could allow for faster optimization of a wireless channel in a changing environment. In the following, we demonstrate resonant structures, a ubiquitous building block for filters, duplexers, multiplexers, and other components in front-end electronics,[12,13] fabricated on a RP film. To understand how material tunability and dielectric loss impact resonator performance, we performed temperature-dependent measurements. The RP film has a paraelectric-ferroelectric phase transition with a Curie temperature near 200 K, so we characterized the resonators at 150 and 200 K in addition to room temperature. Measurements of these components show tuning of ≈20% at 200 K and 2.5% at room temperature for DC tuning voltages of 15 V, and that the tuning timescale of these devices is limited to less than a nanosecond by circuit configuration rather than by the material properties.

Unlike the most common tunable dielectric material, $Ba_x Sr_{1-x} TiO_3$, the $(SrTiO_3)_n SrO$ system remains a viable tunable dielectric with low dielectric loss at frequencies well into the GHz range.[6,10] In contrast to $Ba_x Sr_{1-x} TiO_3$, $(SrTiO_3)_n SrO$ is composed of $SrTiO_3$ layers broken up periodically by $(SrO)_2$ crystallographic shear planes. It is believed that these shear planes accommodate local nonstoichiometry that would otherwise be incorporated as point defects, allowing the active $SrTiO_3$ material between the $(SrO)_2$ layers to remain pristine and thus able to retain low loss into to the gigahertz regime. The $(SrO)_2$ layers act as a low loss, low dielectric constant spacer. In bulk, $(SrTiO_3)_n SrO$ is nonpolar and not tunable. Shown theoretically[11] and proven experimentally,[10] it was found that the application of biaxial tensile strain gives rise to in-plane ferroelectricity, and that the Curie temperature increases with strain
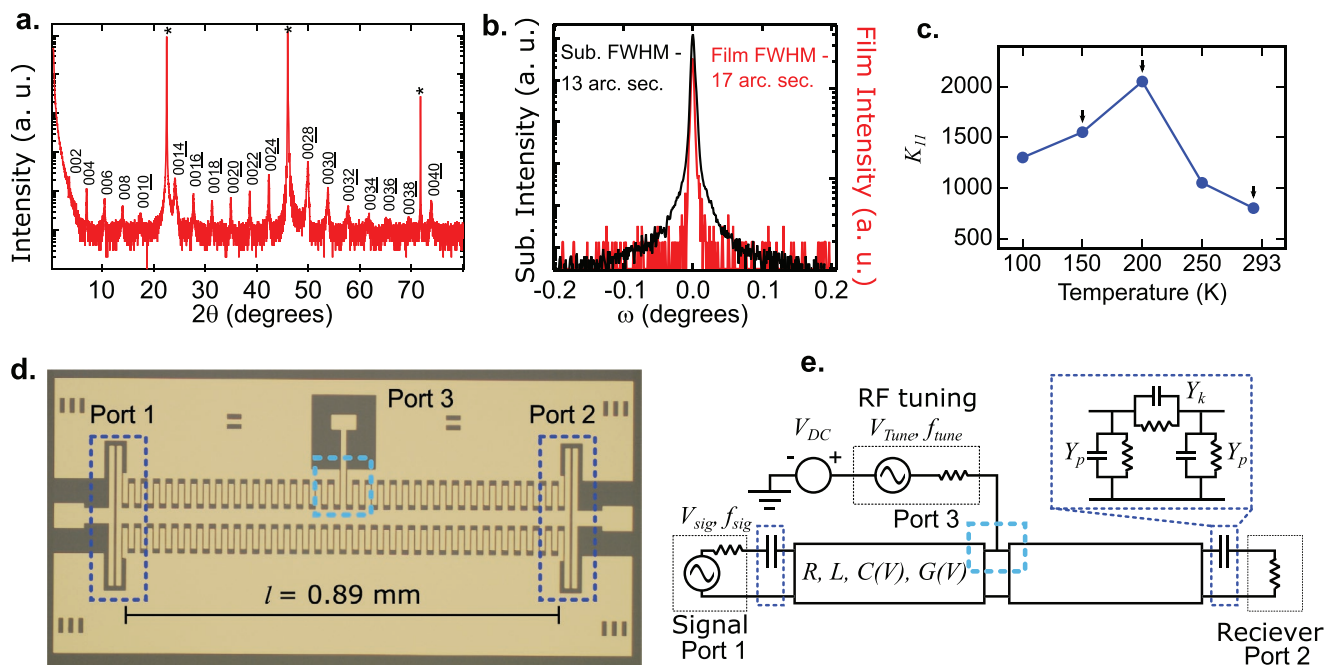
**ADVANCED
SCIENCE NEWS**
www.advancedsciencenews.com

**ADVANCED
MATERIALS
TECHNOLOGIES**
www.advmattechnol.de

Figure 1. A tunable resonator fabricated on 50 nm thick $n = 6$ Ruddlesden–Popper $(SrTiO_3)_6SrO$ thin film on (110) $DyScO_3$ with an analytical compact circuit model. a) θ–2θ XRD characterization of the film. b) Rocking curve data showing high structural quality obtained by MBE deposition. c) Permittivity, K_{11}, as a function of temperature estimated from S-parameter measurements of capacitors and finite element simulation. We see a broad phase transition from ferroelectric to paraelectric states with increasing temperature. Resonator S-parameter and tuning speed measurements were taken at 150, 200, and 293 K. d) Photograph of a lithographically fabricated resonator, showing the three device ports. e) Circuit model of the tunable resonator.

and with the index n of the $(SrTiO_3)_nSrO$ phases. The RPs act as relaxor ferroelectrics due to the $(SrO)_2$ layers breaking up the TiO_2 chains, allowing each $SrTiO_3$ block to act as a nano-domain.[10,11] For tunable dielectrics it is optimal for the Curie temperature to be below, but close to, room temperature to prevent loss due to ferroelectric domain wall motion, while retaining high polarizability. Here, we grow $n = 6$ $(SrTiO_3)_nSrO$ on ScO_2-terminated (110) $DyScO_3$ substrates[12,13] (with lattice constant 3.949 Å) to provide ≈1.1% tensile strain to shift the fer-roelectric Curie temperature to ≈200 K (**Figure 1**c). The film was grown 50 nm thick on (110) $DyScO_3$ using an oxide molecular-beam epitaxy system at a substrate temperature of 875 °C in an oxidant (≈90% O_2 + 10% O_3) background pressure of 1×10^{-4} Pa (1×10^{-6} Torr). The film was found to have high structural per-fection by X-ray diffraction (Figure 1a) and rocking curve scans (Figure 1b). Precise atomic layering was achieved through source shuttering and calibration of individual SrO and TiO_2 monolayers shutter times using reflection high-energy electron diffraction (RHEED) intensity oscillations.[14] Growth was initi-ated by supplying two SrO monolayers to account for the SrO floating layer that remains throughout the deposition.[15,16]

Our resonator consists of a capacitively coupled coplanar-waveguide transmission line that supports resonant standing wave modes (Figure 1d). A high resolution, annotated photo-graph of the resonator is given in Figure S2 (Supporting Information). In general, transmission lines can be modeled using four parameters: a distributed resistance R, inductance L, conductance G, and capacitance C per unit length. A trav-elling wave with angular frequency ω will vary with the posi-tion x along the line as $e^{\gamma x}$, where γ is the propagation constant

given by $\gamma = \alpha + j\beta = \sqrt{(R + j\omega L)(G + j\omega C)}$, and α and β are the attenuation and phase constants, respectively. In the limit that the losses and coupling capacitance are small, the lowest order resonant mode of the device is determined by $\beta\ell = \pi$. At resonance, the voltage is maximum at the ends of the device ($x = 0$ and $x = \ell$), and the current is a maximum at the center. To apply a bias voltage, we added a bias arm in the middle of the resonator (Figure 1d). In the paraelectric state of the RP film (above ≈200 K), a nonzero bias voltage V_{DC} between the center conductor and the outer conductor of the transmission line decreases the permittivity of the RP film. A decreasing per-mittivity decreases the distributed capacitance and shifts the resonance frequency upward, because a higher frequency is needed to satisfy the resonance condition.

In keeping with the requirements of mobile technology, several features of our design allow the resonator to be physi-cally compact (1.160 mm in length). First, we minimized the gap width (the distance between the center conductor and the ground plane) to 2.7 μm to increase the distributed capacitance, and therefore β. We also employed an interdigitated design with 10 μm wide fingers that penetrate 60 μm into the ground plane, further increasing C (Figure 1d). The lowest resonance frequency was between 12 and 15 GHz, depending on the temperature and DC bias. To increase the operating frequency, one can decrease the length of the resonator, increase the gap width, or decrease the length of the interdigitated fingers. We fabricated our tun-able resonators (Figure 1d) on a 10 mm × 10 mm, 50 nm thick $n = 6$ RP film on a (110) $DyScO_3$ substrate by optical lithography. We used a contact aligner to pattern the photoresist, and depos-ited the conductors, consisting of a (5 ± 1) nm titanium adhesion

**ADVANCED
SCIENCE NEWS**

www.advancedsciencenews.com

**ADVANCED
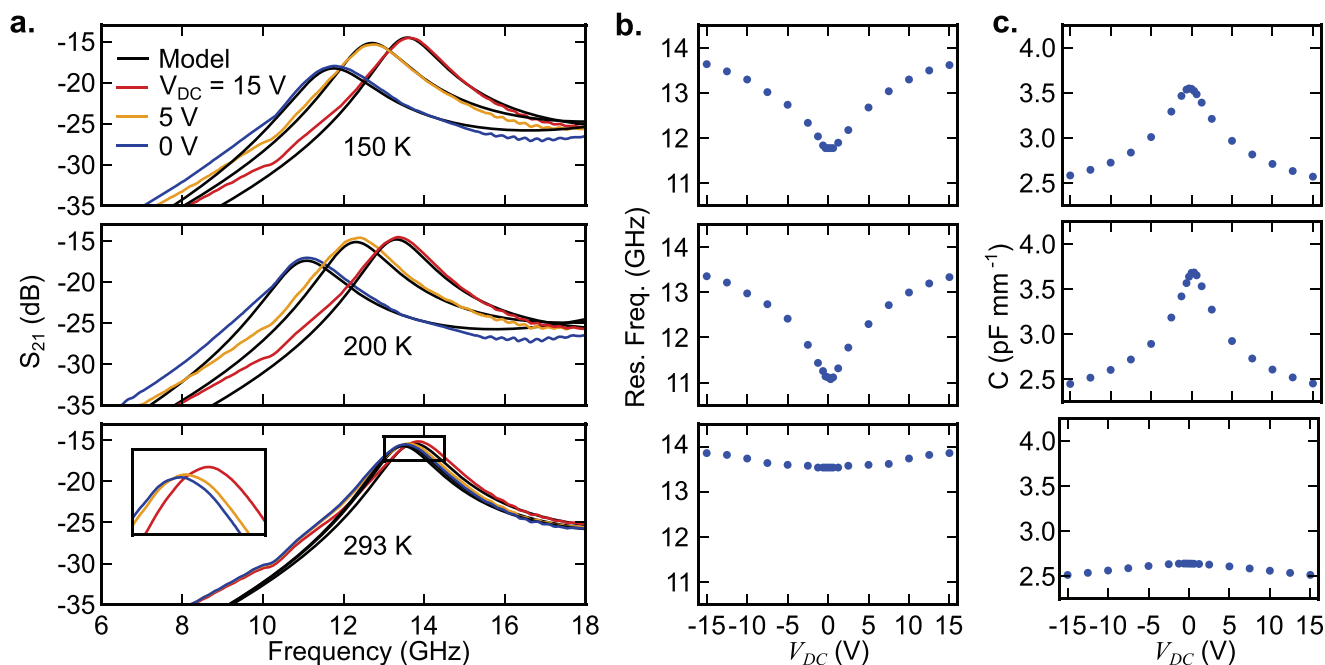MATERIALS
TECHNOLOGIES**

www.advmattechnol.de

Figure 2. Resonator transmission characterization with DC voltage tuning. a) Transmission coefficient, S_{21}, as a function of temperature and bias voltage. A fit to the circuit model is shown as a black line. b). Resonance frequency as a function of bias voltage for the three temperatures measured. c) Distributed capacitance extracted from a fit to the circuit model shown in Figure 1e.

layer followed by a (400 ± 10) nm gold layer, by electron-beam evaporation using a liftoff process to define the structures.

We characterized the linear behavior of our resonator in terms of scattering (S) parameters. The S parameters are defined so that $b_n = \sum_m S_{nm} a_m$, where b_n is the signal leaving the nth port of the device, and a_m is the signal entering the mth port of the device.[17] The quantities $|a|^2$ and $|b|^2$ have dimensions of power, and can be interpreted as the power emitted by a source and the power absorbed by a receiver, respectively. For a 2-port resonator, the parameter (S_{21}) describes the frequency-dependent power transmission and phase shift of the resonator.

Measurements of S_{21} (**Figure 2**a) show a peak in the transmission near the resonance frequency. We measured the transmission as a function of temperature and DC bias voltage V_{DC} in a cryogenic probe station with a vector network analyzer (VNA) and used an on-wafer multiline Thru-Reflect-Line calibration[18] to error-correct the S parameters. The on-wafer calibration standards were fabricated on a LaAlO$_3$ reference substrate. Because this RP film has a Curie temperature of about 200 K, we measured the S parameters at room temperature (paraelectric state), 200, and 150 K (ferroelectric state). At each temperature, V_{DC} was increased from −15 to 15 V. For each bias state, we extracted the resonance frequency (Figure 2b). We observed that the resonance frequency increased with increasing $|V_{DC}|$, and found that this tunability increased near the Curie temperature.

The resonator's static tuning behavior (Figure 2a) can be described by a compact circuit model (see the Supporting Information), where the resonator's tuning behavior was described by the voltage-dependent capacitance per unit length of the waveguide. We extracted C from a fit to the model (the black line in Figure 2a). At a bias voltage of 15 V, C decreased by

≈25, 30, and 4% for 150, 200, and 293 K, respectively; the corresponding increases in the resonance frequencies were ≈15, 20, and 2.5%. We note that the tuning of the capacitance and consequently the resonance frequency could be improved by using thicker films.

In addition to the resonance frequencies, we quantified the loss in the resonator in terms of the parameters of the circuit model. Due to limited space on the chip, we were not able to use the method described in ref. [10] to measure dielectric loss, but we believe this film to have similarly low dielectric loss at room temperature (tan δ ≈ 0.05 at 125 GHz). We quantify the resonator losses by the unloaded quality factor, Q_u,[17] which is the theoretical limiting value of the quality factor as the coupling strength goes to zero. The relative contributions of resistive and dielectric loss can be quantified by Q_c and Q_d, the hypothetical values of Q_u with only resistive loss ($G = 0$) and only dielectric loss ($R = 0$), respectively. Q_c, Q_d, and Q_u are related by $Q_c^{-1} + Q_d^{-1} \approx Q_u^{-1}$.[17] The value of Q_u for these resonators falls in the range of ≈6–10, depending on the temperature and bias voltage. At room temperature, the conductor losses are larger than dielectric losses with $Q_c = 16$, $Q_d = 31$, and $Q_u = 10$ independent of bias voltage. At lower temperatures, the dielectric loss is larger and bias-dependent. At 200 K, Q_d varies from 12 at 0 V_{DC} to 21 at 15 V_{DC}. This bias-dependent loss is also seen in Ba$_x$Sr$_{1-x}$TiO$_3$.[19] The increased dielectric loss near the Curie temperature is a well-known feature of relaxor dielectrics,[20] and has been reported in RP.[10,21] At 150 K, we see a qualitatively similar behavior, with Q_d varying between 9 and 19. We see these trends with bias and temperature reflected in the tuning speed data.

One of the attractive features of voltage-tunable dielectrics is their fast tuning, which is much harder to quantify than the

**ADVANCED
SCIENCE NEWS**
www.advancedsciencenews.com

**ADVANCED
MATERIALS
TECHNOLOGIES**
www.advmattechnol.de

static tunability. One approach is to apply a step-like excitation to a capacitor loaded with the material and measure the time-domain response. Ultrafast optoelectronic methods can measure dynamics on the scale of 10's of ps.[22] Even with fast pulsed lasers and oscilloscopes, interpretation of these experiments is challenging, and both physical- and circuit-level modeling is necessary to separate the contributions of the circuit parameters, material behavior, and the finite rise time of the excitation signal.[23] We argue that small-signal sinusoidal excitation offers a path toward tuning speed characterization which is more general and less dependent on modeling.[24]

Under some very general assumptions, the response of a nonlinear system to two-tone excitation fully determines its behavior under arbitrary excitation in the small signal limit.[25] In the time domain, filters are typically described by a linear, time-invariant transfer function. Such a description is not adequate if the filter's characteristics are modified by a time-varying tuning signal. Equation (1) is a simple generalization of linear theory that relates the incident signal $a_1(t)$, the tuning signal $a_3(t)$, and the output signal $b_2(t)$. The function $K_1(t)$ describes the linear transfer function of the filter and $K_2(t', t'')$ describes how the transfer function is modified by the tuning signal

$$b_2(t) = \int_{-\infty}^{t} dt' K_1(t - t') a_1(t') + \int_{-\infty}^{t} dt' \int_{-\infty}^{t} dt'' K_2(t - t', t - t'') a_3(t') a_1(t'') \quad (1)$$

In Equation (1), $b(t)$ and $a(t)$ have the same physical meaning as they do for S parameters, but are expressed in the time domain rather than the frequency domain. We performed measurements with sinusoidal input signals, so a frequency-domain description is more appropriate

$$b_2(\omega) = S_{21}(\omega) a_1(\omega)$$
$$+ \int_{-\infty}^{\infty} d\omega' \int_{-\infty}^{\infty} d\omega'' \delta(\omega - \omega' - \omega'') \hat{K}_2(\omega', \omega'') a_3(\omega') a_1(\omega'') \quad (2)$$

Equation (2) is mathematically equivalent to Equation (1), but provides a description in terms of quantities that are easier to access experimentally. The linear transfer function of the filter is described by the Fourier transform of $K_1(t)$ in Equation (1), which is also is the scattering parameter $S_{21}(\omega)$. The tuning of the filter is characterized by $\hat{K}_2(\omega', \omega'')$, and the magnitude of this quantity can be inferred from frequency-domain measurements.

The frequency dependence of $\hat{K}_2$ describes the transient tuning behavior in a device. Qualitatively, the function $|\hat{K}_2(\omega_{sig}, \omega_{tune})|^2$, with ω_{sig} held constant, shows a peak where $\omega_{sig} \pm \omega_{tune}$ is at the resonance frequency and the bandwidth of this peak in $\hat{K}_2$ indicates the rate at which tuning transient behavior decays, with a narrower peak corresponding to a longer transient time. Thus, the bandwidth of $\hat{K}_2$ can be used to define a tuning time. To measure $\hat{K}_2$ (Figure 1e), we excite the resonator with a continuous wave signal at a frequency $f_{sig} = 13.25$ GHz (near resonance), with a power of $P_1 = 8$ dBm. We also excited the tuning port with a continuous wave signal at a frequency f_{tune}, which we sweep over a range of frequencies from 6 to 18 GHz. The RF tuning signal had a power of $P_3 = 0$ dBm at the source, and was combined with a DC tuning voltage with a bias tee. Using a spectrum analyzer, we measure

the sideband signals at $f_{sig} \pm f_{tune}$. According to Equation (2), the power of the signal measured at the spectrum analyzer, P_2, is given by $P_2 = |\hat{K}_2(\omega_{sig}, \omega_{tune})|^2 P_3 P_1$. In terms of required equipment, our measurement technique is simple, but still achieves high dynamic range (>70 dB) and a broad bandwidth (18 GHz).

To quantify tuning time, we define $\tau_{10 \text{ dB}} = 1/\Delta_{10 \text{ dB}}$, where $\Delta_{10 \text{ dB}}$ is the full width of the peak in P_2 at 10 dB below the maximum. While this quantity does not directly characterize the time-domain response, it provides information on relevant dynamical timescales, and can be compared over a range of temperatures and voltages. Circuit simulations show that $\tau_{10 \text{ dB}}$ is comparable to the time it takes for transients to decay by 50%, although there is no simple relationship between these two quantities across the range of relevant parameters.

Figure 3a shows the frequency dependences of the sidebands, and Figure 3c shows the dependence of the tuning time on bias voltage and temperature. The circuit takes longer to tune at higher bias voltages and the tuning time is most sensitive to bias voltage at 200 K. These two trends have an intuitive explanation. As we see in the linear data, the dielectric loss is appreciable near the Curie temperature, and decreases with bias voltage. A lower-loss resonator will have a longer transient response to a perturbation or tuning signal compared to a higher-loss resonator, because energy is stored in the resonant mode for a longer time. In order to understand this dependence, we developed a circuit model that accounts for both the nonlinearity of the RP film and the spatial structure of the signals involved (see the Supporting Information). In this model, the small-signal tunability is parameterized by $C'(V_{DC})$, the derivative of the distributed capacitance with respect to the microwave-frequency voltage V when a DC voltage of V_{DC} is applied. Within the resonator, we solve for the voltage and current waves in a transmission line with a voltage-dependent capacitance per unit length, $C(V) = C(V_{DC}) + C'(V_{DC})V$.

Figure 3a shows a comparison between the nonlinear circuit model and the data. There are no fitting parameters to describe the shape of the curve. All of the parameters, except C'/C, are determined by the fit to the S parameters shown in Figure 2a. The model reproduces the shape of the data, including the faster-than-Lorentzian decay of the sideband amplitudes, and the widening due to the offset between the resonance frequency and the signal frequency. The tuning times seen in this model are consistent with those seen in experiment (Figure 3c).

From the circuit model, we expect the sideband voltage to be proportional to C'/C, because the phase of the signal at f_{sig} is modulated by the tuning signal through the variable capacitance per unit length of the device. Since the amplitude of the tuning signal, V_{tune}, is small, the change in propagation constant will be proportional to C'. Indeed, we found that the overall sideband power increased rapidly with V_{DC} when V_{DC} was <2.5 V, consistent with the parabolic dependence of C on V_{DC} for low V_{DC} (Figure 2c). The sideband power also peaks at higher V_{DC}, around 5 V, which is again consistent with the trends seen in the DC tuning (Figure 2c). In contrast to the higher temperatures, at 150 K a relatively strong tuning response is seen at $V_{DC} = 0$ V. Second-order nonlinear effects require a breaking of inversion symmetry. The nonlinear

1800090 (4 of 6)

**ADVANCED
SCIENCE NEWS**
www.advancedsciencenews.com

**ADVANCED
MATERIALS
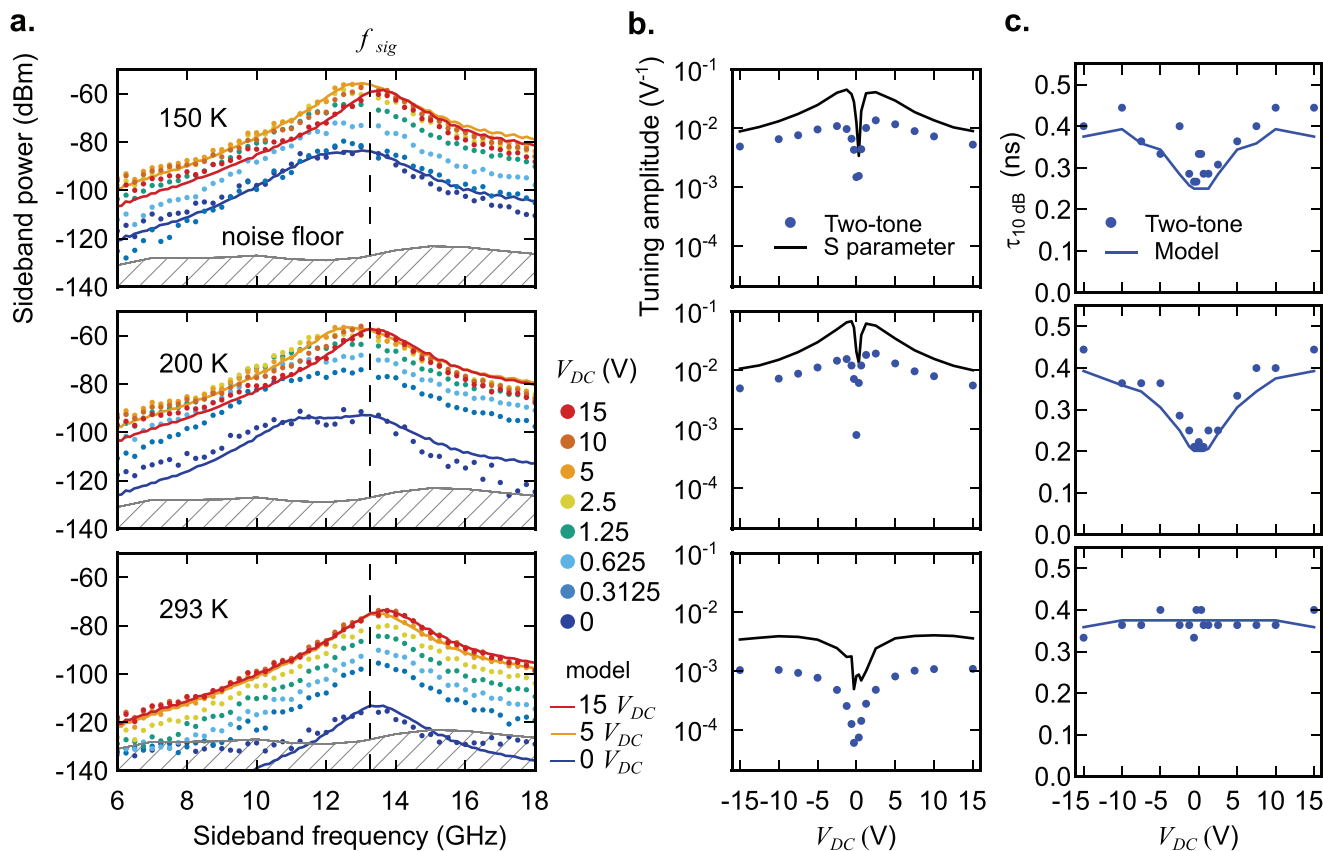TECHNOLOGIES**
www.advmattechnol.de

Figure 3. Resonator tuning speed characterization by two-tone frequency-domain measurements. a) Amplitude of sidebands as a function of tuning frequency, bias voltage, and temperature. The dynamic tuning model is shown for V_{DC} = 0, 5, and 15 V as solid lines. The noise floor is the 95th percentile of measurements with no input signal. b) Comparison of the microwave-frequency tuning amplitude, C'/C calculated from the two-tone measurements with an analogous quantity calculated from S-parameter measurements (Figure 2c). c) The 10-dB tuning time as a function of DC bias voltage, calculated from the two-tone measurements and the tuning model. Tuning time is omitted for V_{DC} = 0 V at 293 K, because the peak is not 10 dB above the noise floor.

response at V_{DC} = 0 V is consistent with remanent polarization in the ferroelectric state, which acts as a source of built-in bias field.

In conclusion, we have shown that compact resonators with a resonance frequency around 12 GHz fabricated on RP films can be tuned over 20% at 200 K, and 2.5% at room temperature by applying a voltage bias. We also introduced a nonlinear measurement scheme to evaluate the tuning speed and formulated a compact model of the device that is consistent with these measurements. The tuning speed measurement demonstrated that the characteristic timescale of the device tuning was less than one nanosecond, showing the feasibility of creating high-tuning-speed phase shifters and filters with RP films. In the model, the device tuning speed is purely due to the linear characteristics of the waveguide and coupling capacitors, while the material's dielectric constant is assumed to change instantaneously in response to an applied bias. This suggests that the intrinsic tuning time of the RP film is well below the subnanosecond tuning time of the device, offering promise for even faster devices. Future work will be focused on reducing the device losses and quantifying the intrinsic tuning speed of the RP films.

Supporting Information

Supporting Information is available from the Wiley Online Library or from the author.

Acknowledgements

Conflict of Interest

The authors declare no conflict of interest.

Keywords

microwave, Ruddlesden–Popper, telecommunications, tunable dielectric, tuning speed

[1] T. S. Rappaport, S. Sun, R. Mayzus, H. Zhao, Y. Azar, K. Wang, G. N. Wong, J. K. Schulz, M. Samimi, F. Gutierrez, *IEEE Access* **2013**, *1*, 335.

[2] W. Roh, J. Y. Seol, J. Park, B. Lee, J. Lee, Y. Kim, J. Cho, K. Cheun, F. Aryanfar, *IEEE Commun. Mag.* **2014**, *52*, 106.

[3] A. Babakhani, X. Guan, A. Komijani, A. Natarajan, A. Hajimiri, *IEEE J. Solid-State Circuits* **2006**, *41*, 2795.

[4] M. Sazegar, Y. Zheng, C. Kohler, H. Maune, M. Nikfalazar, J. R. Binder, R. Jakoby, *IEEE Trans. Antennas Propag.* **2012**, *60*, 5690.

[5] D. Gesbert, M. Shafi, D. Shiu, P. J. Smith, A. Naguib, *IEEE J. Sel. Areas Commun.* **2003**, *21*, 281.

[6] A. K. Tagantsev, V. O. Sherman, K. F. Astafiev, J. Venkatesh, N. Setter, *J. Electroceram.* **2003**, *11*, 5.

[7] J. C. Booth, I. Takeuchi, K.-S. Chang, *Appl. Phys. Lett.* **2005**, *87*, 082908.

[8] S. S. Gevorgian, E. L. Kollberg, *IEEE Trans. Microwave Theory Tech.* **2001**, *49*, 2117.

[9] C. V. Weiss, M. B. Okatan, S. P. Alpay, M. W. Cole, E. Ngo, R. C. Toonen, *J. Mater. Sci.* **2009**, *44*, 5364.

[10] C.-H. Lee, N. D. Orloff, T. Birol, Y. Zhu, V. Goian, E. Rocas, R. Haislmaier, E. Vlahos, J. A. Mundy, L. F. Kourkoutis, Y. Nie, M. D. Biegalski, J. Zhang, M. Bernhagen, N. A. Benedek, Y. Kim, J. D. Brock, R. Uecker, X. X. Xi, V. Gopalan, D. Nuzhnyy, S. Kamba, D. A. Muller, I. Takeuchi, J. C. Booth, C. J. Fennie, D. G. Schlom, *Nature* **2013**, *502*, 532.

[11] T. Birol, N. A. Benedek, C. J. Fennie, *Phys. Rev. Lett.* **2011**, *107*, 257602.

[12] J. E. Kleibeuker, G. Koster, W. Siemons, D. Dubbink, B. Kuiper, J. L. Blok, C.-H. Yang, J. Ravichandran, R. Ramesh, J. E. ten Elshof, D. H. A. Blank, G. Rijnders, *Adv. Funct. Mater.* **2010**, *20*, 3490.

[13] J. E. Kleibeuker, B. Kuiper, S. Harkema, D. H. A. Blank, G. Koster, G. Rijnders, P. Tinnemans, E. Vlieg, P. B. Rossen, W. Siemons, G. Portale, J. Ravichandran, J. M. Szepieniec, R. Ramesh, *Phys. Rev. B* **2012**, *85*, 165413.

[14] J. H. Haeni, C. D. Theis, D. G. Schlom, *J. Electroceram.* **2000**, *4*, 385.

[15] Y. F. Nie, Y. Zhu, C.-H. Lee, L. F. Kourkoutis, J. A. Mundy, J. Junquera, P. Ghosez, D. J. Baek, S. Sung, X. X. Xi, K. M. Shen, D. A. Muller, D. G. Schlom, *Nat. Commun.* **2014**, *5*, ncomms5530.

[16] J. H. Lee, G. Luo, I. C. Tung, S. H. Chang, Z. Luo, M. Malshe, M. Gadre, A. Bhattacharya, S. M. Nakhmanson, J. A. Eastman, H. Hong, J. Jellinek, D. Morgan, D. D. Fong, J. W. Freeland, *Nat. Mater.* **2014**, *13*, 879.

[17] D. M. Pozar, *Microwave Engineering*, Wiley, Hoboken, NJ **2011**.

[18] R. B. Marks, *IEEE Trans. Microwave Theory Tech.* **1991**, *39*, 1205.

[19] R. A. York, *Multifunctional Adaptive Microwave Circuits and Systems*, Scitech Publishing, Raleigh, NC **2009**.

[20] Z. G. Lu, G. Calvarin, *Phys. Rev. B* **1995**, *51*, 2694.

[21] V. Goian, S. Kamba, N. Orloff, T. Birol, C. H. Lee, D. Nuzhnyy, J. C. Booth, M. Bernhagen, R. Uecker, D. G. Schlom, *Phys. Rev. B* **2014**, *90*, 174105.

[22] J. Li, B. Nagaraj, H. Liang, W. Cao, C. H. Lee, R. Ramesh, *Appl. Phys. Lett.* **2004**, *84*, 1174.

[23] J. Li, H. Liang, B. Nagaraj, W. Cao, C. H. Lee, R. Ramesh, *J. Lightwave Technol.* **2003**, *21*, 3282.

[24] A. M. Hagerstrom, E. Marksz, C. J. Long, J. C. Booth, N. D. Orloff, presented at *90th ARFTG Microwave Measurement Symposium (ARFTG)*, Boulder, CO, November **2017**.

[25] J. J. Bussgang, L. Ehrman, J. W. Graham, *Proc. IEEE* **1974**, *62*, 1088.